DISCRETE AND CONTINUOUS
DYNAMICAL SYSTEMS SERIES B
Volume **19**, Number **6**, August **2014**

doi:10.3934/dcdsb.2014.19.1737

pp. **1737–1747**

AN UNCONDITIONALLY STABLE NUMERICAL METHOD FOR THE VISCOUS CAHN–HILLIARD EQUATION

Jaemin Shin

Institute of Mathematical Sciences, Ewha W. University
Seoul 120-750, Republic of Korea

Yongho Choi and Junseok Kim

Department of Mathematics, Korea University
Seoul 136-713, Republic of Korea

(Communicated by Qiang Du)

Abstract. We present an unconditionally stable finite difference method for solving the viscous Cahn–Hilliard equation. We prove the unconditional stability of the proposed scheme by using the decrease of a discrete functional. We present numerical results that validate the convergence and unconditional stability properties of the method. Further, we present numerical experiments that highlight the different temporal evolutions of the Cahn–Hilliard and viscous Cahn–Hilliard equations.

1. **Introduction.** We consider a finite difference scheme for the viscous Cahn–Hilliard (vCH) equation

$$\phi_t(\mathbf{x},t) = \Delta\mu(\mathbf{x},t), \tag{1}$$

$$\mu(\mathbf{x},t) = F'(\phi(\mathbf{x},t)) - \epsilon^2\Delta\phi(\mathbf{x},t) + \nu\phi_t(\mathbf{x},t), \tag{2}$$

where $\Omega \subset \mathbb{R}^d$ $(d = 1, 2, 3)$ is a domain. The quantity $\phi(\mathbf{x}, t)$ is defined as the difference between the concentrations of the two mixture components. $F(\phi) = (\phi^2 - 1)^2/4$ is the Helmholtz free energy, ϵ is the gradient energy coefficient related to the interfacial energy, and ν is the viscosity parameter. The no-flux boundary conditions are

$$\mathbf{n} \cdot \nabla\phi = \mathbf{n} \cdot \nabla\mu = 0 \text{ on } \partial\Omega, \tag{3}$$

where $\mathbf{n}$ is the unit normal vector to $\partial\Omega$. Note that if $\nu = 0$, the vCH equation becomes the Cahn–Hilliard (CH) equation.

The CH equation is a diffuse interface model for describing the spinodal decomposition in binary alloys [3], and the vCH equation is considered as a phenomenological continuum model for phase separation coupling with a slowly relaxing variable [2, 29]. The sharp interface limit of the CH equation is the Mullins–Sekerka model [11, 30]. The viscosity term $\nu\phi_t$ can be interpreted as describing the influences of internal microforces [19]. The mathematical model for the vCH has been derived in [28]. Global existence, solvability, uniqueness, and long-time behavior of the vCH equation have been studied analytically in [4, 9, 10, 13, 17, 26]. Further, the

2010 *Mathematics Subject Classification.* Primary: 65M06, 65M12; Secondary: 65M55.

Key words and phrases. Cahn–Hilliard equation, viscous Cahn–Hilliard equation, unconditionally stable scheme, finite-difference method, multigrid method.

metastable and coarsening dynamics of interfaces for the vCH equation is studied in [32, 33].

The CH equation has been intensively studied using various numerical methods [5, 6, 12, 15, 16, 18, 21, 22, 23, 24, 25, 35, 37]. However, only a small number of authors studied the vCH equation numerically [1, 8, 27, 33]. The main purpose of this paper is to apply the nonlinear splitting method [14, 15] to the vCH equation and prove its unconditional stability. Further, we present numerical experiments that highlight the different dynamics of the CH and vCH equations using the proposed scheme.

This paper is organized as follows. In Section 2, we present the proposed numerical scheme and prove its mass conservation and unconditionally stability. In Section 3, a brief numerical solution procedure is given to condense the discussion. Numerical results are described in Section 4 and conclusions are stated in Section 5.

2. Numerical analysis.

We present a finite difference scheme for the vCH equation and prove the mass conservation and unconditional stability of the numerical scheme. We discretize the vCH equation in a one-dimensional space $\Omega = (a, b)$. Two and three-dimensional discretizations are analogously defined. Let N be a positive even integer, $h = (b-a)/N$ be the uniform mesh size, and $\Omega_h = \{x_i = (i-0.5)h,\ 1 \le i \le N\}$ be the set of cell-centers. Let ϕ_i^n and μ_i^n be the approximations of $\phi(x_i, n\Delta t)$ and $\mu(x_i, n\Delta t)$, respectively, where Δt is the time step. The boundary condition is implemented as

$$\nabla_h \phi^n_{\frac{1}{2}} = \nabla_h \phi^n_{N+\frac{1}{2}} = \nabla_h \mu^n_{\frac{1}{2}} = \nabla_h \mu^n_{N+\frac{1}{2}} = 0, \tag{4}$$

where the discrete differentiation operator is $\nabla_h \phi^n_{i+\frac{1}{2}} = (\phi^n_{i+1} - \phi^n_i)/h$. Then, we define a discrete Laplacian operator by $\Delta_h \phi_i = (\nabla_h \phi^n_{i+\frac{1}{2}} - \nabla_h \phi^n_{i-\frac{1}{2}})/h$ and discrete l_2 inner product by

$$\langle \boldsymbol{\phi}, \boldsymbol{\psi} \rangle_h = h \sum_{i=1}^{N} \phi_i \psi_i, \text{ and } (\nabla_h \boldsymbol{\phi}, \nabla_h \boldsymbol{\psi})_h = h \sum_{i=0}^{N} \nabla_h \phi_{i+\frac{1}{2}} \nabla_h \psi_{i+\frac{1}{2}}, \tag{5}$$

where $\boldsymbol{\phi} = (\phi_1, \phi_2, \cdots, \phi_N)$ and $\boldsymbol{\psi} = (\psi_1, \psi_2, \cdots, \psi_N)$. Further, we define the discrete l_2-norm as $\|\boldsymbol{\phi}\|_2^2 = \langle \boldsymbol{\phi}, \boldsymbol{\phi} \rangle_h$ and the maximum norm as $\|\boldsymbol{\phi}\|_\infty = \max_{1 \le i \le N} |\phi_i|$. By applying a nonlinearly stabilized splitting scheme [14, 15] to vCH, we propose the following scheme:

$$\frac{\phi_i^{n+1} - \phi_i^n}{\Delta t} = \Delta_h \mu_i^{n+1} \tag{6}$$

$$\mu_i^{n+1} = \left(\phi_i^{n+1}\right)^3 - \phi_i^n - \epsilon^2 \Delta_h \phi_i^{n+1} + \nu \frac{\phi_i^{n+1} - \phi_i^n}{\Delta t}, \tag{7}$$

for $i = 1, \cdots, N$. Using boundary conditions (4), we have a discrete summation by parts $\langle \Delta_h \boldsymbol{\phi}, \boldsymbol{\psi} \rangle_h = \langle \boldsymbol{\phi}, \Delta_h \boldsymbol{\psi} \rangle_h = -(\nabla_h \boldsymbol{\phi}, \nabla_h \boldsymbol{\psi})_h$, and the discrete mass conservation is proved by

$$\begin{aligned} \left\langle \boldsymbol{\phi}^{n+1}, \mathbf{1} \right\rangle_h &= \langle \boldsymbol{\phi}^n, \mathbf{1} \rangle_h + \Delta t \left\langle \Delta_h \boldsymbol{\mu}^{n+1}, \mathbf{1} \right\rangle_h \\ &= \langle \boldsymbol{\phi}^n, \mathbf{1} \rangle_h - \Delta t \left(\nabla_h \boldsymbol{\mu}^{n+1}, \nabla_h \mathbf{1} \right)_h = \langle \boldsymbol{\phi}^n, \mathbf{1} \rangle_h, \end{aligned} \tag{8}$$

where $\mathbf{1} = (1, 1, \cdots, 1)$. Next, we prove that schemes (6) and (7) are unconditionally stable. For the case of the CH equation, we refer [25]. First, let us define a discrete

functional

$$\mathcal{E}^h(\boldsymbol{\phi}^n) = \frac{h}{4}\sum_{i=1}^{N}\left((\phi_i^n)^2-1\right)^2 + \frac{\epsilon^2 h}{2}\sum_{i=0}^{N}\left|\nabla_h \phi_{i+\frac{1}{2}}^n\right|^2. \tag{9}$$

We then separate the discrete energy functional $\mathcal{E}^h(\boldsymbol{\phi}^n)$ into three parts:

$$\mathcal{E}^{(1)}(\boldsymbol{\phi}^n) = \frac{h}{2}\left(1+\frac{\nu}{\Delta t}\right)\sum_{i=1}^{N}(\phi_i^n)^2, \tag{10}$$

$$\mathcal{E}^{(2)}(\boldsymbol{\phi}^n) = \frac{\epsilon^2 h}{2}\sum_{i=0}^{N}\left|\nabla_h \phi_{i+\frac{1}{2}}^n\right|^2, \tag{11}$$

$$\mathcal{E}^{(3)}(\boldsymbol{\phi}^n) = h\sum_{i=1}^{N}\left(\frac{(\phi_i^n)^4+1}{4}+\frac{\nu}{2\Delta t}(\phi_i^n)^2\right). \tag{12}$$

Let $\mathcal{E}_c^h(\boldsymbol{\phi}^n) = \mathcal{E}^{(2)}(\boldsymbol{\phi}^n) + \mathcal{E}^{(3)}(\boldsymbol{\phi}^n)$ and $\mathcal{E}_e^h(\boldsymbol{\phi}^n) = \mathcal{E}^{(1)}(\boldsymbol{\phi}^n)$ so that $\mathcal{E}^h(\phi^n) = \mathcal{E}_c^h(\boldsymbol{\phi}^n) - \mathcal{E}_e^h(\boldsymbol{\phi}^n)$. We then define an operator "grad_h" as

$$\mathrm{grad}_h\mathcal{E}^h(\boldsymbol{\phi}^n)_i = -\frac{\Delta_h}{h}\nabla\mathcal{E}^h(\boldsymbol{\phi}^n)_i = -\Delta_h(\phi_i^n)^3 + \Delta_h\phi_i^n + \epsilon^2\Delta_h^2\phi_i^n, \tag{13}$$

where $\Delta_h^2\phi_i = \Delta_h(\Delta_h\phi_i)$ is the discrete biharmonic operator and ∇ is the usual gradient in $\mathbb{R}^N$, i.e.,

$$\nabla\mathcal{E}^h(\boldsymbol{\phi})_i = h\left[(\boldsymbol{\phi}_i)^3 - \boldsymbol{\phi}_i - \epsilon^2\Delta_h\boldsymbol{\phi}_i\right]. \tag{14}$$

For the matrix version of Δ_h, we denote as

$$\Delta_d = \frac{1}{h^2}\begin{pmatrix} -1 & 1 & & & 0 \\ 1 & -2 & 1 & & \\ & \ddots & \ddots & \ddots & \\ & & 1 & -2 & 1 \\ 0 & & & 1 & -1 \end{pmatrix}. \tag{15}$$

Matrix $-\Delta_d$ is the positive semi-definite with eigenvalues

$$\lambda_i = \frac{4}{h^2}\sin^2\frac{(i-1)\pi}{2N}, \tag{16}$$

for $i = 1, \cdots, N$. Let $\mathbf{v}_i = \mathbf{w}_i/|\mathbf{w}_i|$ be the orthonormal eigenvector corresponding to the eigenvalue λ_i, where $\mathbf{w}_i = \left(\cos\frac{(i-1)\pi}{2N}, \cos\frac{3(i-1)\pi}{2N}, \ldots, \cos\frac{(2N-1)(i-1)\pi}{2N}\right)$. For $\mathbf{X}$ and $\mathbf{Y}$ in $\mathbb{R}^N$ such that $\mathbf{X} = \sum_{i=1}^N x_i v_i$ and $\mathbf{Y} = \sum_{i=1}^N y_i v_i$, we define

$$\langle \mathbf{X}, \mathbf{Y}\rangle_{-1,h} := h\sum_{i=2}^{N}\lambda_i^{-1}x_i y_i. \tag{17}$$

We note that for $\mathbf{X}$ and $\mathbf{Y}$ such that $x_1 = 0$ or $y_1 = 0$, we have the identity

$$\langle \mathbf{X}, \mathbf{Y}\rangle_h = h\sum_{i=2}^{N}x_i y_i = h\sum_{i=2}^{N}\lambda_i^{-1}\lambda_i x_i y_i = \langle -\Delta_d\mathbf{X}, \mathbf{Y}\rangle_{-1,h}. \tag{18}$$

We can rewrite schemes (6) and (7) in terms of a gradient of the discrete functional $\mathcal{E}^h(\boldsymbol{\phi})$ as

$$\frac{\phi_i^{n+1}-\phi_i^n}{\Delta t} = -\mathrm{grad}_h\mathcal{E}_c^h(\boldsymbol{\phi}^{n+1})_i + \mathrm{grad}_h\mathcal{E}_e^h(\boldsymbol{\phi}^n)_i, \tag{19}$$

for $i = 1, \cdots, N$. The Hessian of $\mathcal{E}^{(1)}(\boldsymbol{\phi})$, denoted by $\mathbf{H}^{(1)}$, is the Jacobian of $\nabla\mathcal{E}^{(1)}(\boldsymbol{\phi})$ and therefore, it is given by

$$\mathbf{H}^{(1)} = \nabla^2\mathcal{E}^{(1)}(\boldsymbol{\phi}) = h\left(1 + \frac{\nu}{\Delta t}\right) I_N, \tag{20}$$

the Hessian matrix of $\mathcal{E}^{(2)}(\boldsymbol{\phi})$ is given as

$$\mathbf{H}^{(2)} = \nabla^2\mathcal{E}^{(2)}(\boldsymbol{\phi}) = -h\epsilon^2\Delta_d \tag{21}$$

and the Hessian matrix of $\mathcal{E}^{(3)}(\boldsymbol{\phi})$ is given as

$$\begin{aligned}\mathbf{H}^{(3)} &= \nabla^2\mathcal{E}^{(3)}(\boldsymbol{\phi}) = 3h\begin{pmatrix}\phi_1^2 & & & & 0\\ & \phi_2^2 & & & \\ & & \ddots & & \\ & & & \phi_{N-1}^2 & \\ 0 & & & & \phi_N^2\end{pmatrix} + \frac{\nu}{\Delta t+\nu}\mathbf{H}^{(1)}\\ &:= 3h\mathbf{D} + \frac{\nu}{\Delta t+\nu}\mathbf{H}^{(1)},\end{aligned} \tag{22}$$

where we have used Eq. (4). The eigenvalues of $\mathbf{H}^{(1)}$ and $\mathbf{H}^{(2)}$ are

$$\lambda_i^{(1)} = h\left(1 + \frac{\nu}{\Delta t}\right), \tag{23}$$

$$\lambda_i^{(2)} = \frac{4\epsilon^2}{h}\sin^2\frac{(i-1)\pi}{2N}, \tag{24}$$

for $i = 1, 2, \cdots, N$. The eigenvalues of $\mathbf{D}$ are non-negative since ϕ_i^2 are non-negative. Then, the eigenvalues of $\mathbf{H}^{(3)}$ are non-negative from the Weyl's Theorem [20]:

$$\lambda_i^{(3)} \geq \lambda_i(\mathbf{D}) + \frac{\nu}{\Delta t+\nu}\lambda_1^{(1)} \geq 0. \tag{25}$$

Note that $\lambda_i^{(1)}$, $\lambda_i^{(2)}$, and $\lambda_i^{(3)}$ are non-negative for all i. Let $\boldsymbol{\phi}^{n+1} - \boldsymbol{\phi}^n$ be expressed in terms of $\mathbf{v}_i$ as

$$\boldsymbol{\phi}^{n+1} - \boldsymbol{\phi}^n = \sum_{i=1}^{N}\alpha_i\mathbf{v}_i. \tag{26}$$

If $\boldsymbol{\phi}^{n+1}$ is the solution of Eqs. (6) and (7) with given $\boldsymbol{\phi}^n$, then

$$\mathcal{E}^h(\boldsymbol{\phi}^{n+1}) \leq \mathcal{E}^h(\boldsymbol{\phi}^n). \tag{27}$$

We now prove the inequality (27). With an exact Taylor expansion of $\mathcal{E}^h(\boldsymbol{\phi}^n)$ about $\boldsymbol{\phi}^{n+1}$ up to second order, we have

$$\begin{aligned}\mathcal{E}^h\left(\boldsymbol{\phi}^n\right) &= \mathcal{E}^h\left(\boldsymbol{\phi}^{n+1}\right) + \left\langle\frac{1}{h}\nabla\mathcal{E}^h(\boldsymbol{\phi}^{n+1}), \boldsymbol{\phi}^n - \boldsymbol{\phi}^{n+1}\right\rangle_h\\ &\quad + \left\langle\frac{1}{2h}\nabla^2\mathcal{E}^h(\boldsymbol{\xi})(\boldsymbol{\phi}^n - \boldsymbol{\phi}^{n+1}), \boldsymbol{\phi}^n - \boldsymbol{\phi}^{n+1}\right\rangle_h,\end{aligned} \tag{28}$$

where $\boldsymbol{\xi} = \theta\boldsymbol{\phi}^n + (1-\theta)\boldsymbol{\phi}^{n+1}$ and $0 \leq \theta \leq 1$. By the discrete mass conservation and the definition of $\mathbf{v}_i$, we have $0 = \left\langle\boldsymbol{\phi}^n - \boldsymbol{\phi}^{n+1}, \mathbf{1}\right\rangle_h = -\sum_{i=1}^{N}\alpha_i\langle\mathbf{v}_i, \mathbf{1}\rangle_h = -h\sqrt{N}\alpha_1$, and therefore $\alpha_1 = 0$. Now from Eq. (18), we have the identity

$$\left\langle\frac{1}{h}\nabla\mathcal{E}^h(\boldsymbol{\phi}^{n+1}), \boldsymbol{\phi}^n - \boldsymbol{\phi}^{n+1}\right\rangle_h = \left\langle\mathrm{grad}_h\mathcal{E}^h(\boldsymbol{\phi}^{n+1}), \boldsymbol{\phi}^n - \boldsymbol{\phi}^{n+1}\right\rangle_{-1,h}. \tag{29}$$

Using Eq. (29), we rearrange Eq. (28)

$$\begin{aligned}\mathcal{E}^h(\boldsymbol{\phi}^{n+1}) - \mathcal{E}^h(\boldsymbol{\phi}^n) &= \left\langle \mathrm{grad}_h \mathcal{E}^h(\boldsymbol{\phi}^{n+1}), \boldsymbol{\phi}^{n+1} - \boldsymbol{\phi}^n \right\rangle_{-1,h} \\ &\quad -\frac{1}{2h}\left\langle \nabla^2 \mathcal{E}^h(\boldsymbol{\xi})(\boldsymbol{\phi}^{n+1} - \boldsymbol{\phi}^n), \boldsymbol{\phi}^{n+1} - \boldsymbol{\phi}^n \right\rangle_h . \end{aligned} \tag{30}$$

For the first term of Eq. (30), using the mean value theorem and Eqs. (19) and (29), we have

$$\begin{aligned}&\left\langle \mathrm{grad}_h \mathcal{E}^h(\boldsymbol{\phi}^{n+1}), \boldsymbol{\phi}^{n+1} - \boldsymbol{\phi}^n \right\rangle_{-1,h} \\ =\ & \left\langle \mathrm{grad}_h \mathcal{E}_c^h(\boldsymbol{\phi}^{n+1}) - \mathrm{grad}_h \mathcal{E}_e^h(\boldsymbol{\phi}^{n+1}), \boldsymbol{\phi}^{n+1} - \boldsymbol{\phi}^n \right\rangle_{-1,h} \\ & - \left\langle \frac{\boldsymbol{\phi}^{n+1} - \boldsymbol{\phi}^n}{\Delta t} + \mathrm{grad}_h \mathcal{E}_c^h(\boldsymbol{\phi}^{n+1}) - \mathrm{grad}_h \mathcal{E}_e^h(\boldsymbol{\phi}^n), \boldsymbol{\phi}^{n+1} - \boldsymbol{\phi}^n \right\rangle_{-1,h} \\ \leq\ & - \left\langle \mathrm{grad}_h \mathcal{E}_e^h(\boldsymbol{\phi}^{n+1}) - \mathrm{grad}_h \mathcal{E}_e^h(\boldsymbol{\phi}^n),\ \boldsymbol{\phi}^{n+1} - \boldsymbol{\phi}^n \right\rangle_{-1,h} \\ =\ & - \left\langle \frac{1}{h}\nabla \mathcal{E}_e^h(\boldsymbol{\phi}^{n+1}) - \frac{1}{h}\nabla \mathcal{E}_e^h(\boldsymbol{\phi}^n), \boldsymbol{\phi}^{n+1} - \boldsymbol{\phi}^n \right\rangle_h \\ =\ & - \left\langle \frac{1}{h}\nabla^2 \mathcal{E}_e^h(\boldsymbol{\eta})\left(\boldsymbol{\phi}^{n+1} - \boldsymbol{\phi}^n\right), \boldsymbol{\phi}^{n+1} - \boldsymbol{\phi}^n \right\rangle_h \\ =\ & -\frac{1}{h}\left\langle \mathbf{H}^{(1)}\left(\boldsymbol{\phi}^{n+1} - \boldsymbol{\phi}^n\right), \boldsymbol{\phi}^{n+1} - \boldsymbol{\phi}^n \right\rangle_h , \end{aligned} \tag{31}$$

where $\boldsymbol{\eta} = \theta\boldsymbol{\phi}^n + (1-\theta)\boldsymbol{\phi}^{n+1}$ and $0 \leq \theta \leq 1$. For the second term of Eq. (30), using $\mathcal{E}^h = -\mathcal{E}^{(1)} + \mathcal{E}^{(2)} + \mathcal{E}^{(3)}$, we have

$$\begin{aligned}& -\frac{1}{2h}\left\langle \nabla^2 \mathcal{E}^h(\boldsymbol{\xi})(\boldsymbol{\phi}^{n+1} - \boldsymbol{\phi}^n), \boldsymbol{\phi}^{n+1} - \boldsymbol{\phi}^n \right\rangle_h \\ =\ & \frac{1}{2h}\left\langle \left(\mathbf{H}^{(1)} - \mathbf{H}^{(2)} - \mathbf{H}^{(3)}\right)(\boldsymbol{\phi}^{n+1} - \boldsymbol{\phi}^n), \boldsymbol{\phi}^{n+1} - \boldsymbol{\phi}^n \right\rangle_h \\ \leq\ & \frac{1}{2h}\left\langle \mathbf{H}^{(1)}(\boldsymbol{\phi}^{n+1} - \boldsymbol{\phi}^n), \boldsymbol{\phi}^{n+1} - \boldsymbol{\phi}^n \right\rangle_h . \end{aligned} \tag{32}$$

From inequalities (31) and (32),

$$\begin{aligned}\mathcal{E}^h(\boldsymbol{\phi}^{n+1}) - \mathcal{E}^h(\boldsymbol{\phi}^n) &\leq -\frac{1}{2h}\left\langle \mathbf{H}^{(1)}(\boldsymbol{\phi}^{n+1} - \boldsymbol{\phi}^n), \boldsymbol{\phi}^{n+1} - \boldsymbol{\phi}^n \right\rangle_h \\ &= -\frac{1}{2}\left(1 + \frac{\nu}{\Delta t}\right)\left\|\boldsymbol{\phi}^{n+1} - \boldsymbol{\phi}^n\right\|_h^2 \leq 0. \end{aligned} \tag{33}$$

Therefore, we have proven the decrease of the discrete functional $\mathcal{E}^h$ for any time step Δt. Moreover, the decrease of the discrete functional $\mathcal{E}^h$ implies the pointwise boundedness of the numerical solution; $\|\boldsymbol{\phi}^n\|_\infty \leq \sqrt{1 + 2\sqrt{\mathcal{E}^h(\boldsymbol{\phi}^0)/h}}$ for all n [24]. Therefore, we deduce that the proposed numerical scheme is unconditionally stable.

3. **Numerical solution.** We use a multigrid method [34] to solve the governing discretized system (6) and (7) at the implicit time level. To condense the discussion, we describe only the relaxation step for the multigrid method. A pointwise Gauss–Seidel relaxation is used as the smoother in the multigrid method. To derive the nonlinear system, let us define it as

$$N\left(\phi^{n+1}, \mu^{n+1}\right) = \left(\varphi^n, \psi^n\right), \tag{34}$$

where the nonlinear system operator N is

$$N(\phi^{n+1}, \mu^{n+1}) = \left(\frac{\phi^{n+1}}{\Delta t} - \Delta_d \mu^{n+1},\ \mu^{n+1} - \left(\phi^{n+1}\right)^3 + \epsilon^2 \Delta_d \phi^{n+1} - \nu \frac{\phi^{n+1}}{\Delta t} \right) \quad (35)$$

and the source term is $(\varphi^n, \psi^n) = (\phi^n/\Delta t, -\phi^n - \nu\phi^n/\Delta t)$. For more details, refer [36].

4. **Numerical results.** In this section, we perform numerical experiments for the convergence test, linear stability analysis, unconditional stability test, and convexity preservation. If we consider that the concentration field varies from -0.9 to 0.9 over the interfacial region with m grid points, the value ϵ is defined by $\epsilon_m = hm/(2\sqrt{2}\tanh^{-1}(0.9))$.

4.1. **Convergence test.** Tables 1 and 2 summarize the discrete l_2 and maximum norms of errors and the convergence rates for space and time. For the simulation, the initial condition is used as $\phi(x, 0) = 0.1\cos(2\pi x)$ in the computational domain $\Omega = (0, 1)$. For the other parameters, $\epsilon = 0.03$ and $\nu = 0.01$ are used. Because no analytical solutions are available, we use the relative error to calculate the convergence rate. The spatial convergence rate is measured using mesh grids with $N = 2^n$ for $n = 5, 6, 7, 8$. Numerical solutions are computed up to time $T = 0.1$ with the time step size $\Delta t = 10^{-7}$. We define the error of a grid as the difference between the grid and the average of the next finer grid cells as follows: $e_i^h := \phi^h(x_i, T) - \left(\phi^{h/2}(x_{2i-1}, T) + \phi^{h/2}(x_{2i}, T)\right)/2$. The rate of convergence is defined as the ratio of successive errors, $\log_2(\|e^h\|_2/\|e^{h/2}\|_2)$. The second-order accuracy of space is observed as expected (Table 1).

TABLE 1. Errors and convergence rates for space.

Mesh	32	Rate	64	Rate	128	Rate	256
$\|e^h\|_2$	7.793e-3	2.095	1.823e-3	2.014	4.515e-4	2.003	1.126e-4
$\|e^h\|_\infty$	1.602e-2	1.878	4.358e-3	1.967	1.115e-3	1.994	2.799e-4

To show the convergence of time integration, we fix the spatial grid as $N = 512$ and choose a set of time steps $\Delta t = 2^n \times 10^{-7}$, for $n = 0$, 1, 2, and 3. In addition, we run the computation up to time $T = 0.1$. Note that we define the discrete error as $e_i^{\Delta t} := \phi^{\Delta t}(x_i, T) - \phi^{\Delta t/2}(x_i, T)$. The rate of convergence is defined as the ratio of successive errors, $\log_2(\|e^{\Delta t}\|_2/\|e^{\Delta t/2}\|_2)$. Table 2 indicates that the scheme is first-order accurate in time.

TABLE 2. Errors and convergence rates for time.

Δt	8e-7	Rate	4e-7	Rate	2e-7	Rate	1e-7
$\|e^{\Delta t}\|_2$	8.739e-9	1.000	4.369e-9	1.000	2.185e-9	0.999	1.093e-9
$\|e^{\Delta t}\|_\infty$	2.804e-7	1.000	1.402e-7	1.000	7.012e-8	0.999	3.508e-8

4.2. **Linear stability analysis.** We conduct the linear stability analysis near an equilibrium solution $\phi = 0$ in a one-dimensional space. Let us assume that the solution can be expressed by

$$\phi(x,t) = \sum_{k=1}^{\infty} \beta_k(t) \cos(kx), \tag{36}$$

where $\beta_k(t)$ is an amplification factor at the wave number k. After linearizing Eqs. (1) and (2) about the equilibrium solution, and substituting Eq. (36) into the linearized equations, we have

$$\frac{d\beta_k(t)}{dt} = \frac{k^2\left(1-\epsilon^2 k^2\right)}{1+\nu k^2}\beta_k(t). \tag{37}$$

The solution of Eq. (37) is $\beta_k(t) = \beta_k(0)\exp(\eta_k t)$, where $\eta_k = k^2(1-\epsilon^2k^2)/(1+\nu k^2)$ is the growth rate. Note that the growth rate is positive if $\epsilon k < 1$. We denote $k_{\max}$ by the wave number that has the maximal growth rate. In addition, the numerical growth rate is defined by $\widetilde{\eta}_k = \log(\|\boldsymbol{\phi}^n\|_\infty/\|\boldsymbol{\phi}^0\|_\infty)/T$. For the numerical test, we consider the initial condition $\phi(x,0) = 0.01\cos(kx)$ in $\Omega = (0,\pi)$. Numerical simulations are run up to $T = 10^{-6}$ with $\Delta t = 10^{-8}$, $h = 2^{-9}\pi$, and $\epsilon = 0.03$.

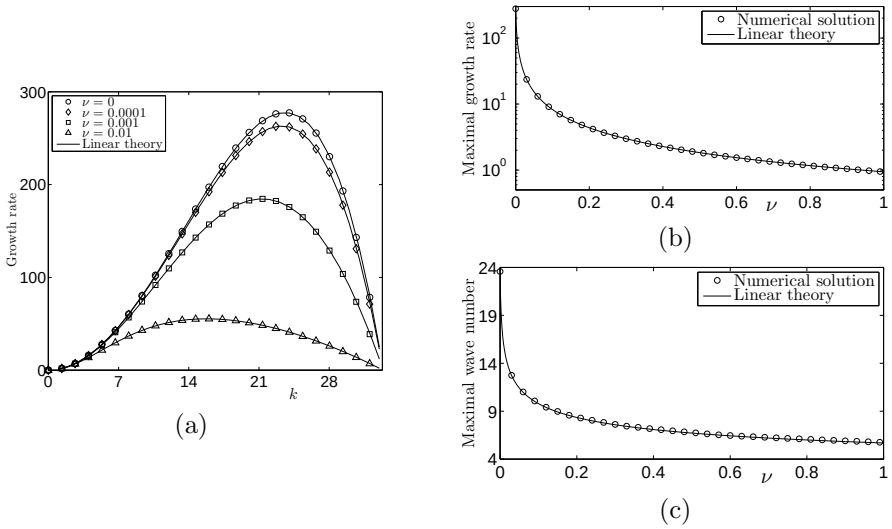

FIGURE 1. (a) Growth rate versus the wave number k. (b) maximal growth rate and (c) maximal wave number versus the viscosity ν. Symbols are from the numerical computations and the solid lines are from the linear stability analysis.

Figure 1(a) illustrates the growth rate $\widetilde{\eta}_k$ versus the wave number k with different viscosities ν. Solid lines correspond to analytic solutions from linear stability analysis. Figures 1(b) and 1(c) compare the theoretical and numerical results for the maximal growth rate $\eta_{k_{\max}}$ and maximal wave number $k_{\max}$, respectively. To numerically compute $\eta_{k_{\max}}$ and $k_{\max}$, a quadratic interpolation is applied. The numerical results and analytic values are in good agreement. Both the maximal wave number $k_{\max}$ and maximal growth rate $\eta_{k_{\max}}$ tend to rapidly decrease with increasing viscosity ν.

4.3. **Unconditional stability test.** To demonstrate the unconditional stability of the proposed scheme, we consider the initial data that is a random perturbation of the state $\phi = 0$ with values distributed uniformly between -0.1 and 0.1. $\Omega = (0,1) \times (0,1)$, $h = 1/64$, ϵ_4, and $\nu = 1$ are considered. Figure 2 shows numerical results after ten iterations with three different temporal steps $\Delta t = 1$, 10, and 100. The results suggest that the proposed scheme is unconditionally stable.

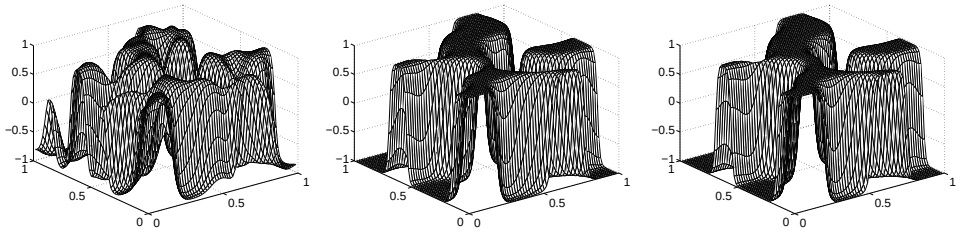

(a) $\Delta t = 1$ (b) $\Delta t = 10$ (c) $\Delta t = 100$

FIGURE 2. Snapshots after ten iterations with different time steps

4.4. **Convexity preservation.** We investigate the evolutions of the CH and vCH equations with an initially convex shape in $\Omega = (0, 02) \times (0, 0.005)$. The initial condition is $\phi(x, y, 0) = \tanh(d(x, y)/(\sqrt{2}\epsilon_6))$, where

$$d(x,y) = \begin{cases} 0.001 - \sqrt{(x-0.0075)^2 + (y-0.0025)^2} & \text{if } x \le 0.0075, \\ 0.001 - \sqrt{(x-0.0125)^2 + (y-0.0025)^2} & \text{if } x \ge 0.0125, \\ -|y-0.0025| + 0.001 & \text{otherwise.} \end{cases} \tag{38}$$

$h = 0.01/64$, $\Delta t = 10^{-6}$, and ϵ_6 are used. Figure 3 plots the minimum of the curvature, $\kappa = \nabla \cdot (-\nabla\phi/|\nabla\phi|)$, on the interface $\phi = 0$ against the scaled time t/T, where $T = 2.045\text{e-}5$, 2.145e-5, 3.019e-5, and 9.077 for the viscosity $\nu = 0$, 1e-7, 1e-6, and 1, respectively. The readers may refer to [22] for the numerical evaluation of κ at the cell centers. Then, we use a bilinear interpolation to compute the curvature values on the interface $\phi = 0$ from the cell center data. The numerical minimum curvature shows negative values for the CH equation ($\nu = 0$) at early evolutions. However, with increased viscosity, the minimum value of curvature along the interface increases.

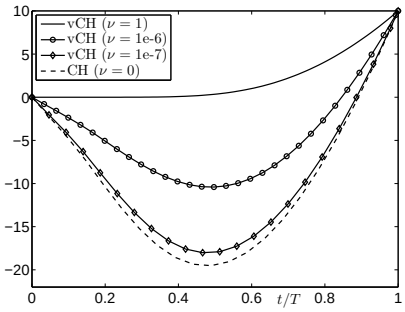

FIGURE 3. Minimum curvature with different viscosities

4.5. **Boundedness of solution.** We consider the following question [31]: If an initial ϕ has values in $[-1, 1]$, does the solution of Eqs. (1) and (2) have values in $[-1, 1]$ at all times? The authors in [7] rigorously answered for the question. Here, we are interested in the numerical stationary solutions of the CH and vCH equations for the same initial condition. We define $\boldsymbol{\phi}^{n+1}$ is the steady state if $\|\boldsymbol{\phi}^{n+1} - \boldsymbol{\phi}^n\|_\infty < 10^{-9}$. The initial condition is sphere (Fig. 4(a)), which is defined as

$$\phi(x, y, z, 0) = \tanh\left(\frac{0.25 - \sqrt{(x-0.5)^2 + (y-0.5)^2 + (z-0.5)^2}}{\sqrt{2}\epsilon}\right) \tag{39}$$

in $\Omega = (0, 1) \times (0, 1) \times (0, 1)$. For the numerical parameters, $h = 1/64$, $\Delta t = 0.1h$, $\epsilon = 0.0169$, and $\nu = 1$ are used. Figure 4(b) shows a slice plot of the steady states along the line $y = z = 0.5$. We can observe that both steady state solutions are identical and $\|\boldsymbol{\phi}\|_\infty > 1$ inside the drop. This result suggests that $\|\boldsymbol{\phi}\|_\infty > 1$ is due to the curvature effect. For the CH equation case, these shrinkage phenomena were also observed in [37].

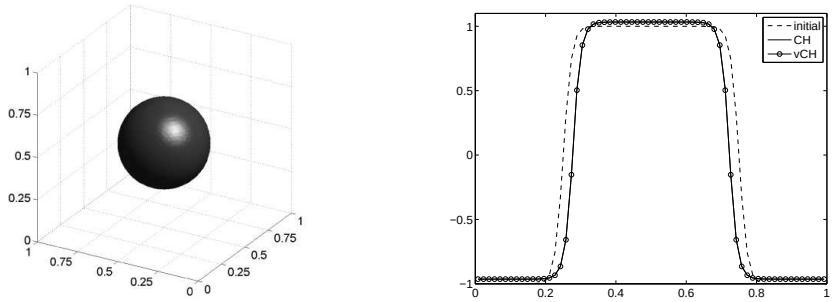

(a) (b)

FIGURE 4. (a) Initial condition and (b) slice plots ($y = z = 0.5$) of the steady state solutions of CH and vCH equations with $\nu = 1$.

5. **Conclusions.** We proposed an unconditionally stable scheme for the viscous Cahn–Hilliard equation based on the finite difference method. We proved the unconditional stability, and it was confirmed through numerical experiments with large time step sizes. Linear stability analysis showed that the solution of the viscous Cahn–Hilliard equation decays more slowly than that of the Cahn–Hilliard equation. The difference between the Cahn–Hilliard and viscous Cahn–Hilliard equations was illustrated by examining various numerical experiments.

Acknowledgments. The corresponding author (J.S. Kim) is supported by Basic Science Research Program through the National Research Foundation of Korea (NRF) funded by the Ministry of Education (NRF-2011-0023794). The author (J. Shin) is supported by Basic Science Research Program through the National Research Foundation of Korea (NRF) funded by the Ministry of Education (2009-0093827). The authors thank the reviewers for their valuable suggestions and comments that significantly improved the quality of this paper.

REFERENCES

[1] F. Bai, C. M. Elliott, A. Gardiner, A. Spence and A. M. Stuart, The viscous Cahn–Hilliard equation. Part I: Computations, *Nonlinearity,* **8** (1995), 131–160.

[2] K. Binder, H. L. Frisch and J. Jäckle, Kinetics of phase separation in the presence of slowly relaxing structural variables, *J. Chem. Phys.,* **85** (1986), 1505–1512.

[3] J. W. Cahn and J. E. Hilliard, Free energy of a nonuniform system. I. Interfacial free energy, *J. Chem. Phys.,* **28** (1958), 258–267.

[4] A. N. Carvalho and T. Dlotko, Dynamics of the viscous Cahn–Hilliard equation, *J. Math. Anal. Appl.,* **344** (2008), 703–725.

[5] R. Chella and J. Viñals, Mixing of a two-phase fluid by cavity flow, *Phys. Rev. E.,* **53** (1996), 3832–3840.

[6] L. Q. Chen and J. Shen, Applications of semi-implicit Fourier-spectral method to phase field equations, *Comput. Phys. Commun.,* **108** (1998), 147–158.

[7] L. Cherfils, A. Miranville and S. Zelik, The Cahn–Hilliard equation with logarithmic potentials, *Milan J. Math.,* **79** (2011), 561–596.

[8] S. M. Choo, S. K. Chung and Y. J. Lee, A conservative difference scheme for the viscous Cahn–Hilliard equation with a nonconstant gradient energy coefficient, *Appl. Numer. Math.,* **51** (2004), 207–219.

[9] P. Colli, G. Gilardi, P. Podio-Guidugli and J. Sprekels, An asymptotic analysis for a nonstandard Cahn–Hilliard system with viscosity, *Discrete Contin. Dyn. Syst. Ser. S,* **6** (2013), 353–368.

[10] P. Colli, G. Gilardi, P. Podio-Guidugli and J. Sprekels, Well-posedness and long-time behavior for a nonstandard viscous Cahn–Hilliard system, *SIAM J. Appl. Math.,* **71** (2011), 1849–1870.

[11] S. Dai and Q. Du, Motion of interfaces governed by the Cahn–Hilliard equation with highly disparate diffusion mobility, *SIAM J. Appl. Math.,* **72** (2012), 1818–1841.

[12] Q. Du and R. A. Nicolaides, Numerical analysis of a continuum model of phase transition, *SIAM J. Numer. Anal.,* **28** (1991), 1310–1322.

[13] C. M. Elliott and A. M. Stuart, Viscous Cahn–Hilliard equation II. Analysis, *J. Differential Equations,* **128** (1996), 387–414.

[14] D. J. Eyre, *An Unconditionally Stable One-Step Scheme for Gradient Systems*, Unpublished article, **http://www.math.utah.edu/∼eyre/research/methods/stable.ps** (1998).

[15] D. J. Eyre, Unconditionally gradient stable time marching the Cahn–Hilliard equation, *Mater. Res. Soc. Symp. Proc.,* **529** (1998), 39–46.

[16] D. Furihata, A stable and conservative finite difference scheme for the Cahn–Hilliard Equation, *Numer. Math.,* **87** (2001), 675–699.

[17] C. G. Gal and M. Grasselli, Singular limit of viscous Cahn–Hilliard equations with memory and dynamic boundary conditions, *Discrete Contin. Dyn. Syst. Ser. B,* **18** (2013), 1581–1610.

[18] H. Gómez, V. M. Calo, Y. Bazilevs and T. J. Hughes, Isogeometric analysis of the Cahn–Hilliard phase-field model, *Comput. Methods Appl. Mech. Engrg.,* **197** (2008), 4333–4352.

[19] M. Gurtin, Generalized Ginzburg–Landau and Cahn–Hilliard equations based on a microforce balance, *Phys. D,* **92** (1996), 178–192.

[20] R. A. Horn and C. R. Johnson, *Matrix Analysis*, Cambridge Univ. Press, London, 1985.

[21] D. Kay and R. Welford, A multigrid finite element solver for the Cahn–Hilliard equation, *J. Comput. Phys.,* **212** (2006), 288–304.

[22] J. Kim, A continuous surface tension force formulation for diffuse-interface models, *J. Comput. Phys.,* **204** (2005), 784–804.

[23] J. Kim, A numerical method for the Cahn–Hilliard equation with a variable mobility, *Commun. Nonlinear. Sci. Numer. Simulat.,* **12** (2007), 1560–1571.

[24] J. Kim, Phase-field models for multi-component fluid flows, *Commun. Comput. Phys.,* **12** (2012), 613–661.

[25] J. S. Kim and H. O. Bae, An unconditionally gradient stable adaptive mesh refinement for the Cahn–Hilliard equation, *J. Korean Phys. Soc.,* **53** (2008), 672–679.

[26] D. Li and X. Ju, On dynamical behavior of viscous Cahn–Hilliard equation, *Discret. Contin. Dyn. Syst.,* **32** (2013), 2207–2221.

[27] S. Momani and V. S. Erturk, A numerical scheme for the solution of viscous Cahn–Hilliard equation, *Numer. Meth. Part. D. E.,* **24** (2008), 663–669.

[28] A. Novick-Cohen, On the viscous Cahn–Hilliard equation, Material Instabilities in Continuum and Related Mathematical Problems, *Oxford Univ. Press,* New York, (1988), 329–342.

[29] A. Novick–Cohen, The Cahn–Hillard equation: Mathematical and modeling perspectives, *Adv. Math. Sci. Appl.,* **8** (1998), 965–985.
[30] R. L. Pego, Front migration in the nonlinear Cahn–Hilliard equation, *Proc. R. Soc. Lond. A. Math. Phys. Sci.,* **422** (1989), 261–278.
[31] M. Pierre, Uniform convergence for a finite-element discretization of a viscous diffusion equation, *J. Numer. Anal.,* **30** (2010), 487–511.
[32] L. G. Reyna and M. Ward, Metastable internal layer dynamics for the viscous Cahn–Hilliard equation, *Methods and Appl. of Anal.,* **2** (1995), 285–306.
[33] X. Sun and M. Ward, Dynamics and coarsening of interfaces for the viscous Cahn–Hilliard equation in one spatial dimension, *Stud. Appl. Math.,* **105** (2000), 203–234.
[34] U. Trottenberg, C. Oosterlee and A. Schüller, *Multigrid*, Academic press, London, 2001.
[35] B. P. Vollmayr-Lee and A. D. Rutenberg, Fast and accurate coarsening simulation with an unconditionally stable time step, *Phys. Rev. E.,* **68** (2003), 066703, 13pp.
[36] S. D. Yang, H. G. Lee and J. S. Kim, A phase-field approach for minimizing the area of triply periodic surfaces with volume constraint, *Comput. Phys. Commun.,* **181** (2010), 1037–1046.
[37] P. Yue, C. Zhou and J. J. Feng, Spontaneous shrinkage of drops and mass conservation in phase-field simulations, *J. Comput. Phys.,* **223** (2007), 1–9.

Received November 2013; 1st revision November 2013; 2nd revision March 2014.

E-mail address: jmshin@ewha.ac.kr
E-mail address: poohyongho@korea.ac.kr
E-mail address: cfdkim@korea.ac.kr